

# Nanoparticle size threshold for magnetic agglomeration and associated hyperthermia performance

D. Serantes<sup>1,\*</sup> and D. Baldomir<sup>1</sup>

<sup>1</sup>*Applied Physics Department and Instituto de Investigaciones Tecnológicas,  
Universidad de Santiago de Compostela, 15782 Santiago de Compostela, Spain*

The likelihood of magnetic nanoparticles to agglomerate is usually estimated through the ratio between magnetic dipole-dipole and thermal energies, thus neglecting the fact that, depending on the magnitude of the magnetic anisotropy constant ( $K$ ), the particle moment may fluctuate internally and thus undermine the agglomeration process. Based on the comparison between the involved timescales, we study in this work the threshold size for magnetic agglomeration of magnetite-like nanoparticles in terms of  $K$ , and the associated heating performance. Our results suggest that agglomeration is prevented up to sizes in the range  $\sim 16 - 20$  nm in diameter, for  $K$  in the range  $15 \text{ kJ/m}^3$  down to  $8 \text{ kJ/m}^3$ . Remarkably, the different particles (in terms of  $K$  and size) are predicted to have a very similar large heating performance. An analysis comparing the agglomeration predictions with usual *superparamagnetism* estimations is provided, as well as with the energy competition approach.

## I. INTRODUCTION

Based on the possibility to achieve local actuation by a harmless remote magnetic field, magnetic nanoparticles are very attractive candidates for novel medical applications [1, 2]. Particularly iron oxides, based on their good biocompatibility [3], have been the subject of intense research in recent years, for example for magnetic hyperthermia cancer therapy [4, 5] or drug release [6, 7].

A key aspect to consider when dealing with magnetic nanoparticles for biomedical applications is the agglomeration likelihood, as it could affect not only the metabolising process but also the magnetic properties by changing the interparticle interactions [8]. Considering for example magnetic hyperthermia, it is known that the particles tend to agglomerate when internalized by the cells and that such may lead to a decrease of the heating performance [9]. However, the opposite behaviour has also been reported, with an increase of the heat release if the particles form chains [10]. In general, accounting for the effect of interparticle dipolar interactions is of primary importance for a successful application [11].

The complex role of the interparticle interactions often prompts researchers to the use of *superparamagnetic* (SPM) particles, with the idea that the rapid internal fluctuation of the particles' magnetic moments shall prevent their agglomeration. Thus, in first approximation one could be tempted to consider that agglomeration will not occur for particles with blocking temperature ( $T_B$ ) below the desired working temperature, since for  $T > T_B$  the particles are in the SPM state (i.e. they behave paramagnetic-like). However, it must be kept in mind that behaving SPM-like is not an absolute term, but it is defined by the experimental timescale. Thus, regarding agglomeration, a particle could be referred to as SPM if its Néel relaxation time,  $\tau_N$ , is smaller than the characteristic timescales that allow agglomeration, i.e. diffusion ( $\tau_{diff}$ ) and rotation ( $\tau_B$ ) [12]. These are given by

$$\tau_N = \frac{\sqrt{\pi}}{2} \tau_0 \frac{e^{\frac{KV}{k_B T}}}{\left(\frac{KV}{k_B T}\right)^{\frac{1}{2}}}, \quad (1)$$

$$\tau_{diff} = \frac{x^2 6\pi\eta R_{hyd}}{k_B T}, \quad (2)$$

and

$$\tau_B = \frac{3\eta V_{hyd}}{k_B T}, \quad (3)$$

respectively, where  $\tau_0 = 10^{-9}$  s,  $K$  is the uniaxial anisotropy constant and  $V$  the particle volume;  $k_B$  is the Boltzmann constant,  $x$  the particle diffusion distance, and  $\eta$  the viscosity of the embedding media;  $R_{hyd}$  and  $V_{hyd}$  are the hydrodynamic radius and volume, respectively, defined as the particle size plus a nonmagnetic coating of thickness  $t_{nm}$ .

The objective of this work is to estimate the size threshold for magnetic agglomeration,  $d_{aggl}$  (i.e. size for which  $\tau_N > \tau_{diff}, \tau_B$ , so that agglomeration is likely) in terms of  $K$ . Particularly we will focus on magnetite based on its primary importance for bioapplications. For the sake of generality we will consider different values of the *effective* uniaxial anisotropy  $K$ , which can be ascribed to dominance of shape anisotropy over the magnetocrystalline one [13, 14]. The results will be compared with the predictions of the parameter usually applied to estimate the agglomeration likelihood, i.e. the ratio between the dipolar energy of parallel-aligned moments of touching particles and thermal energy [15, 16]:

$$\Gamma = \frac{\mu_0 (M_S V)^2}{2\pi d^3 k_B T}, \quad (4)$$

where  $\mu_0 = 1.256 * 10^{-6} \text{ Tm/A}$  is the permeability of free space,  $M_S$  the saturation magnetization, and  $d$  the center to center interparticle distance. Note that eq. (4) does not consider  $K$ , despite its key role in the agglomeration probability. Then, the hyperthermia performance for the obtained  $d_{aggl}$  will be studied. It must be recalled here the double role of  $K$  in the heating performance, as it determines both the maximum achievable heating [17, 18] and the effectiveness in terms of field amplitude [19]; for completeness, this double role of  $K$  in heating will also be briefly summarized. Please note that we are using "agglomeration" referring to a *reversible* process, distinct from the *irreversible* "aggregation" [20].

\* E-mail: david.serantes@usc.gal

## II. RESULTS AND DISCUSSION

### A. Size threshold for magnetic agglomeration, $d_{aggl}$

To estimate  $d_{aggl}$  we followed the same approach as we did in Ref. [12]: to compare the characteristic Néel, diffusion, and rotation times, and define  $d_{aggl}$  as the size for which  $\tau_N > \tau_{diff}, \tau_B$ . The particle saturation magnetization is taken fixed as  $M_S = 4.8 * 10^5$  A/m, i.e. the upper value for real systems so that the interaction is, most likely, overestimated. We considered three values of the uniaxial anisotropy constant:  $K = 8, 11,$  and  $15$  kJ/m<sup>3</sup>, i.e. values of the order found in the literature [12, 21, 22]. The diffusion distance in eq. (2) is set as the interparticle distance at which the magnetostatic energy dominates over the thermal one, i.e.  $\Gamma > 1$  [12], but setting at first the thickness of the nonmagnetic coating ( $t_{nm}$ ) to zero, so that interactions are maximized:

$$x = \left( \frac{\mu_0 (M_S V)^2}{2\pi k_B T} \right)^{\frac{1}{3}}. \quad (5)$$

While we have chosen  $\Gamma = 1$  to have a well defined criterion, agglomeration usually requires higher  $\Gamma$  values [23]. That is to say, we are searching for the lower  $d_{aggl}$  boundary. For the viscosity we used  $\eta = 0.00235$  kg/m\*s, as in Ref. [24], which is comparable to that of HeLa cells for nm-scale dimensions [25]. The relaxation times as a function of the particle diameter,  $d$ , are shown in Figure 1.

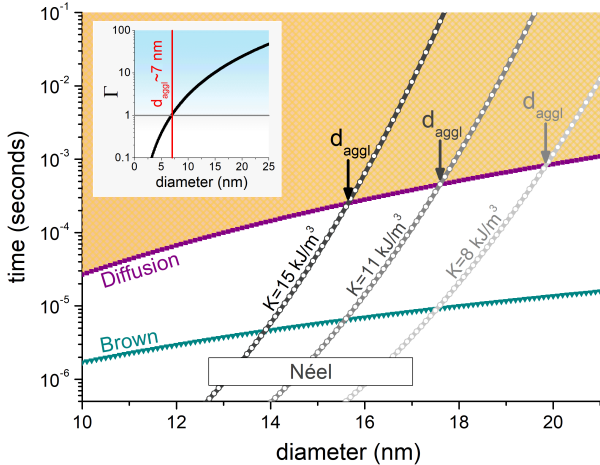


FIG. 1. Diffusion ( $\tau_{diff}$ ; purple line), Brown ( $\tau_B$ ; green line), and Néel relaxation time ( $\tau_N$ ; grey lines), as a function of the particle diameter. The distinct  $\tau_N$  curves correspond to the different  $K$  values indicated. The dashed light-orange area indicates the range where agglomeration can be expected. The inset shows the size dependence of the  $\Gamma$ , which predicts agglomeration for sizes  $d > 7$  nm.

In Figure 1 it is clearly observed how increasing  $K$  leads to more stable moments, thus favouring agglomeration at smaller sizes (from  $d_{aggl} \sim 20$  nm for  $K = 8$  kJ/m<sup>3</sup>, to  $d_{aggl} \sim 16$  nm for  $K = 15$  kJ/m<sup>3</sup>). The inset shows the size dependence of the  $\Gamma$ ,

the  $\Gamma$  value of eq. (4), which i) does not distinguish among particle characteristics (in terms of  $K$ , as previously mentioned), and; ii) predicts dominance of the dipolar energy for much smaller particle sizes, with  $d_{aggl} \sim 7$  nm. It is worth noting that the threshold value obtained for the  $K = 11$  kJ/m<sup>3</sup> case,  $d_{aggl} \approx 18$ , is significantly smaller than the one previously reported in Ref. [12] (for which  $d_{aggl} \approx 21$  nm). Such difference is mainly due to larger  $M_S$  value used here in order to reach the ideal situation, which significantly enhances the diffusion time (through the diffusion distance, eq. (5)). The fact that so far we are not considering a nonmagnetic coating has a minor effect, as discussed next.

While we considered  $t_{nm} = 0$  in order to determine the boundary where clustering might appear, biomedical applications will always require a biocompatible nonmagnetic coating and therefore it is important to consider its role. That being said, the analysis shows that including a non-magnetic coating does not significantly modify the obtained threshold values: if considering  $t_{nm} = 5$  nm,  $d_{aggl}$  increases just by  $\sim 0.2$  nm; and by  $\sim 0.5$  nm if  $t_{nm} = 20$  nm. This is illustrated in Figure 2A.

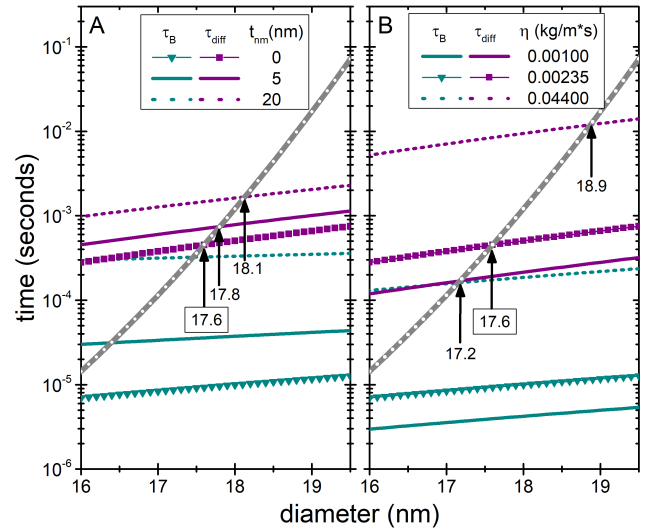


FIG. 2. Diffusion ( $\tau_{diff}$ ; purple line), Brown ( $\tau_B$ ; green line), and Néel relaxation time ( $\tau_N$ ; grey line), as a function of the particle diameter, as in Figure 1, but considering different thickness of the nonmagnetic coating (left A panel), or viscosity of the medium (right B panel). For simplicity, the results are focused on the  $K = 11$  kJ/m<sup>3</sup> and the original curves from Figure 1 are reproduced for guidance. The variations of  $t_{nm}$  and  $\eta$  are shown with solid and dotted lines, for the values displayed within each panel. The arrows and attached numbers indicate  $t_{aggl}$ , with the reference one (17.6 nm) highlighted.

A slightly larger influence is that of the viscosity of the embedding media, as illustrated in Figure 2B. Considering for example that of water,  $\eta = 0.001$  kg/m\*s, it is observed a 0.4 nm decrease from the average size. This value of viscosity is very significant because of being very similar to that of the cells cytoplasm, although it must be kept in mind that large variations can be observed within the same cell type and among different types of cells [26]. A much higher viscosity would

have a more significant effect, as illustrated for example with the macroscopic value of HeLa cells,  $\eta = 0.044 \text{ kg/m}^3\text{s}$ ; nevertheless this values would be unrealistically high for the current particle sizes, as such large  $\eta$  would correspond to much bigger particle sizes (over  $\sim 86 \text{ nm}$  for HeLa cells) because of the size-dependent viscosity at the microscale [25].

It is important to note that for the anisotropy values considered here, in all cases the size threshold  $d_{aggl}$  is always defined by the competition between diffusion and Néel times, as  $\tau_B < \tau_{diff}$  for all cases shown in Figure 2.

Next we will compare the predictions from the relaxation times with those obtained from *zero field cooling/field cooling* (ZFC/FC) measurements, the common way to estimate SPM behaviour (and thus likely non-agglomeration). If associating the onset of SPM behaviour to the blocking temperature, estimated as  $T_B = KV/25k_B$  [27], the corresponding threshold  $d_{T_B}$  is readily obtained. Thus, the comparison between the agglomeration thresholds predicted by both approaches at room temperature (i.e. setting  $T_B = 300 \text{ K}$ ) is summarized in Table I.

TABLE I. Agglomeration size thresholds obtained through the relaxation times approach ( $d_{aggl}$ ) and through the ZFC/FC one ( $d_{T_B}$ ), at room temperature for the three anisotropy cases of Figure 1.

$K(\text{kJ/m}^3)$	$d_{aggl}(\text{nm})$	$d_{T_B}(\text{nm})$
8	19.8	29.2
11	17.6	26.2
15	15.6	23.6

The comparison between the  $d_{aggl}$  and  $d_{T_B}$  values in Table I shows the latter ones to be -on average- about  $\sim 8.7 \text{ nm}$  bigger than the predicted from the relaxation times approach. In fact, the obtained  $d_{T_B}$  values correspond to a lower boundary, as they were estimated considering the limit case of no applied field, which is not possible in real ZFC/FC experiments. In general, applying the field during the measurements will result in lower  $T_B$  [28–30], which would correspond to larger  $d_{T_B}$  (at least for the monodisperse case considered here; polydispersity might result in more complex scenarios [31–33]).

### B. Associated heating performance

Similar to its importance on the agglomeration likelihood, the anisotropy plays a principal role in defining the hyperthermia performance. On the one hand, it defines the maximum energy that can be dissipated [4, 34]: it is easy to see that for aligned easy axes the maximum hysteresis losses *per loop* are  $8K$  [35] ( $2K$  for the random easy axes distribution [18]). On the other hand, it settles the response to the applied field (of amplitude  $H_{max}$ ) through the anisotropy field, defined as  $H_K = 2K/\mu_0 M_S$  [19, 34]. This double key-role is illustrated in Figure 3, where the heating performance is reported in terms of the usual *Specific Absorption Rate* parameter, SAR, as  $SAR = A * f$ , where  $A$  stands for the area of the loop (hysteresis losses), and  $f$  is the frequency of the AC field.

The simulations were performed in the same way as in Ref. [12]: we considered a random dispersion of monodisperse non-interacting nanoparticles (with the easy axes directions also randomly distributed), and simulated their response under a time varying magnetic field by using the standard Landau-Lifshitz-Gilbert equation of motion within the OOMMF software package [36]; for the random thermal noise (to account for finite temperature) we used the extension module *thetaevolve* [37].

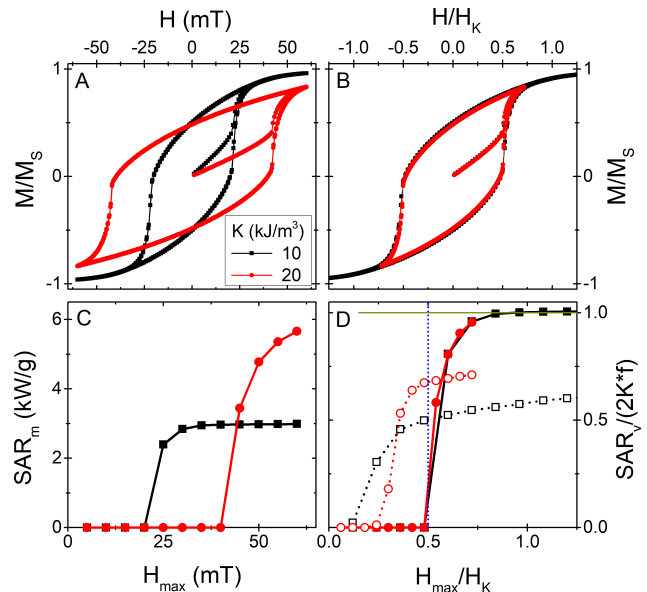


FIG. 3. A: Illustrative  $M$  vs.  $H$  hysteresis loops of two systems of particles of same size ( $d = 20 \text{ nm}$ ) and  $M_S = 480 \text{ kA/m}$ , but different  $K$  ( $10$  and  $20 \text{ kJ/m}^3$ , respectively), at  $T = 0 \text{ K}$  and for  $H_{max} = 25 \text{ mT}$ . B: Same data as in A, replotted in terms of  $H/H_K$ . C: SAR vs.  $H_{max}$  for the two different particles, for  $f = 765 \text{ kHz}$ , at  $T = 0 \text{ K}$ . D: Same data as in panel C, replotted in terms of  $SAR/2K * f$  and  $H/H_K$ ; the curves with open symbols correspond to the  $T = 300 \text{ K}$  case. The vertical blue dotted line stands for the  $\sim 0.5H_K$  threshold of the random distribution [34], and the horizontal solid dark-yellow line indicates the normalized maximum  $SAR/(2K * f) = 1$  limit case.

The results displayed in Figure 3 show how, same as the apparently different hysteresis loops (A panel) are scaled by the anisotropy field (B panel), the apparently different SAR vs.  $H_{max}$  trends scale if plotting  $SAR/(2K * f)$  vs.  $H_{max}/H_K$  (the  $2f$  factor is just for normalisation). Note, however, that those results correspond to the Stoner-Wohlfarth-like case at  $T = 0 \text{ K}$ . In real systems with finite temperature,  $K$  also defines -as previously discussed- the stability of the magnetization within the particle. Thus, the ideal  $T = 0 \text{ K}$  situation may vary significantly due to the effect of thermal fluctuations, as shown by the open symbols in Figure 3D, which correspond to the  $T = 300 \text{ K}$  case for the two particle types considered. It is clearly observed how the strict  $H_{max} \sim 0.5H_K$  threshold does not hold, and that the SAR is much smaller than the maximum possible.

The results shown in Figure 3 illustrate well the the double role of the anisotropy on the heating performance. What is

more, it must be kept in mind that the magnetic anisotropy is the only reason why small particles, such as the ones considered here of typical hyperthermia experiments (well described by the *macrospin* approximation) release heat under the AC field: *if no anisotropy were to exist, there would be no heating* (at least not for the frequencies and fields considered). This applies both to Néel and Brown heating, as with no anisotropy the magnetization would not transfer torque to the particle for its physical reorientation. Of course, larger sizes could display different heating mechanisms (due to non-coherent magnetization behaviour [38] or even eddy currents [39]), but that is not the present case.

We will analyse now the hyperthermia properties of the obtained threshold sizes for the different  $K$  values. Since the roles of surface coating and media viscosity are not very significant in relation to  $d_{aggl}$ , we have focused, for simplicity, on the  $K$  and  $d_{aggl}$  values summarized on Table I, which would set an ideal limit. Thus, we simulated the dynamic hysteresis loops for the three cases considered, to then evaluate the heating capability. Some representative hysteresis loops are shown in Figure 4.

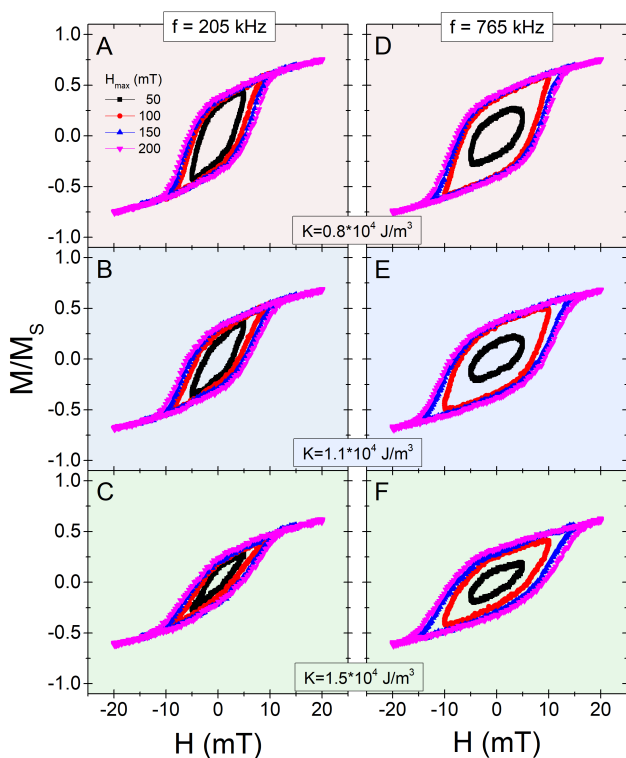


FIG. 4.  $M(H)$  hysteresis loops, for different  $H_{max}$  values, as indicated by the labels in panel A. Left and right columns correspond to  $f = 205$  and  $765$  kHz, respectively. Each pair of colour panels corresponds to a different  $K$  value (indicated within the figure), and for each case the particle size is the corresponding  $d_{aggl}$  from Figure 1.

The results displayed in Figure 4 are very similar for all cases. The most significant differences are that the loops are wider for the  $f = 765$  kHz case, and that with increasing

anisotropy the loops are more sheared. This is due to the fact that larger anisotropy requires higher fields to open the loops due to the minor-major loops competition [18, 19], as illustrated in Figure 3A. Next we will discuss the associated SAR values, which are shown in Figure 5.

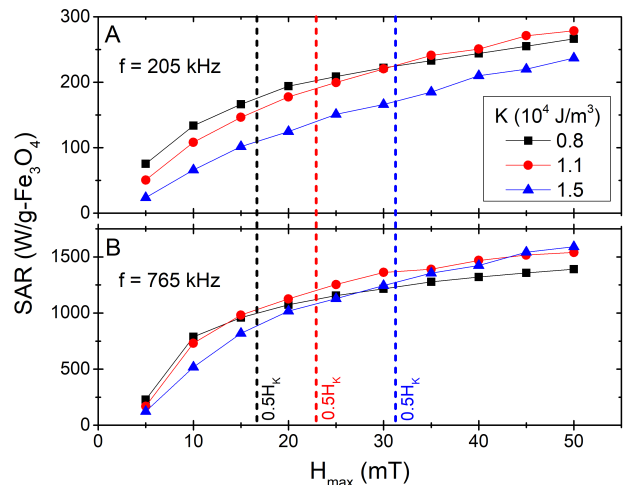


FIG. 5. SAR vs.  $H_{max}$  for the three  $K$  values (at corresponding  $d_{aggl}$ ), for  $f = 205$  and  $765$  kHz. The vertical lines stand for half of the anisotropy field of each  $K$  value (of same colour).

The results shown in Figure 5 indicate a similar field dependence for the different particles, with very comparable values for the high frequency case and just a slightly superior heating for the lower-K particles for the low frequency one. The absence of a significant change at  $\sim 0.5H_K$  (vertical dotted lines) indicates that the system behaviour is far from that of Stoner-Wohlfarth-like particles [18, 40]. This aspect may be interesting in the sense of reducing the variability in *local* heating effects due to size or anisotropy polydispersity [19, 41]), as the difference between *blocked* and SPM particles would be the highest [19, 42]. The results are also clearly divergent from the *linear response theory* model [24], for which  $SAR \propto H_{max}^2$ ; this is not surprising as we are far from its applicability conditions (see e.g. Refs. [43, 44] for a detailed discussion).

The predicted SAR values are quite large, which would make those types of particles efficient heat mediators. However, it is important to recall here the implications of a key ideal assumption we made: the interparticle distance for which the magnetostatic energy would favour agglomeration was obtained from eq. 5. That is to say, no considerations about sample concentration were made. While this may appear reasonable in a first approach, the fact is that the sample concentration is a key parameter to determine, since the amount of particles not only defines the amount of deliverable heat, but also because interparticle interactions (even without agglomeration) may significantly change the heating performance [34, 45].

Thus, to provide some hint on how the sample concentration volume fraction,  $c$ , relates to the assumption made, we



have introduced it through the equivalent nearest-neighbors interparticle distance,  $l_{NN}$ . Following Tewari and Gokhale [46], for a randomly distribution of monodisperse particles we can approximate  $l_{NN}$  as [18]

$$l_{NN} = d \cdot \frac{0.4465}{c^{1/3}} \left[ 1 + 1.02625 \left( \frac{c}{0.64} \right)^{2/3} \right]. \quad (6)$$

Thus, we can use eq. 6 to obtain the sample concentration for which the agglomeration threshold previously discussed applies,  $c_{aggl}$ , just by comparing with the agglomeration distance obtained from eq. 5. This is shown in Figure 6 for the  $K = 1.1 \times 10^4 \text{ J/m}^3$  case as an example.

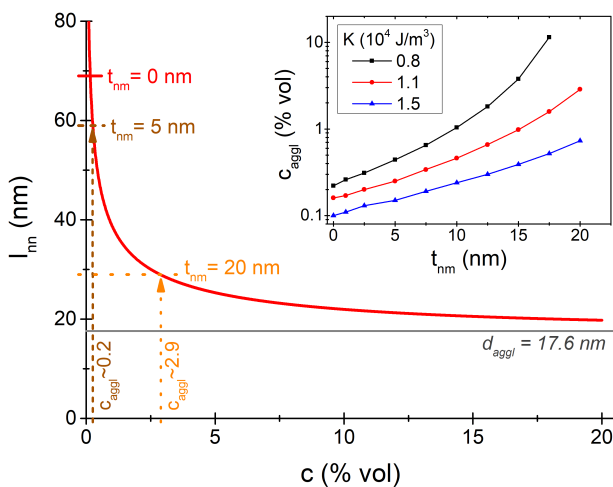


FIG. 6. Nearest-neighbours distance,  $l_{NN}$ , vs. sample volume concentration,  $c$ . The short (coloured) horizontal lines indicate the interparticle distance predicted by eq. 5 for three cases of nonmagnetic coating thickness,  $t_{nm}$ . The vertical arrows indicate the corresponding concentration threshold for agglomeration,  $c_{aggl}$ . The large grey horizontal line indicates the  $d_{aggl}$  value for the  $K = 1.1 \times 10^4 \text{ J/m}^3$  case, to which  $l_{NN}$  tends asymptotically. The inset shows  $c_{aggl}$  vs.  $t_{nm}$  for the three values of  $K$  considered.

The results shown in Figure 6 indicate that for bare uncoated particles ( $t_{nm} = 0 \text{ nm}$ ), the applicability of the discussed arguments would be limited to very small concentrations, of  $c_{aggl} \sim 0.2\%$ . However, in this case the nonmagnetic coating is shown to play a quite significant role in extending  $c_{aggl}$ , as illustrated in the main panel for the cases of  $t_{nm} = 5$  and  $20 \text{ nm}$ . Furthermore, what is shown to play a decisive role here is the anisotropy: smaller anisotropies extend the applicability of our arguments on the size threshold for agglomeration to significantly higher concentrations (see inset). At this point it is worth noting that for iron oxides it has been reported the existence of an essentially non-interacting regime at low concentrations [47, 48], characteristically very attractive from the application viewpoint.

### III. CONCLUSIONS

We have presented an estimation of the threshold sizes for magnetic agglomeration of magnetite-like nanoparticles, depending on their magnetic anisotropy. Our approach was based on the consideration that  $K$  determines the stability of the particle magnetization and thus the likelihood of magnetic agglomeration, which involves physical translation and rotation of the particles themselves. By comparing the associated timescales, we have obtained that magnetite particles with usual anisotropy values should be relatively stable against agglomeration up to sizes in the range  $\sim 16 - 20 \text{ nm}$  in diameter. Then, we evaluated the associated hyperthermia performance, and found it to be relatively large (hundreds of  $\text{W/g}$ ) for usual field/frequency conditions. The role of the nonmagnetic surface coating and that of the media viscosity appears secondary in determining the threshold sizes for agglomeration.

The initial considerations were made with no considerations about sample concentration, despite being a critical parameter for the application. In this regard, simple estimates indicate that the assumptions would be strictly valid only for very diluted conditions. However, the presence of a nonmagnetic coating might significantly extend the validity of the approximations to higher concentrations (up to about  $10\%$  volume fraction), showing that in this sense the nonmagnetic coating would play a key role.

Finally, it is important to recall that we have focused here on purely *magnetic* agglomeration, not considering the role of e.g. electrostatics, which may play an important role [49, 50]; as well as other important system characteristics as polydispersity in size (both regarding aggregation [12] and heating [41]), and in anisotropy. The latter is expected to play a key role based on its primary importance both for agglomeration and heating, as discussed here. However, to the best of our knowledge its role has only been investigated regarding heating performance [19], but not regarding agglomeration likelihood. Considering the combined influence of those parameters clearly constitutes a challenging task for future works. It is also worthy to mention that while we have focused on magnetite-like parameters as a representative example, for simplicity we have assumed the characteristic  $K$  and  $M_S$  values to be independent of size and temperature; the accurate determination of the agglomeration likelihood and hyperthermia performance of a specific system would require including also those dependencies, in addition to the aforementioned system parameters.

### IV. ACKNOWLEDGEMENTS

The authors acknowledge invaluable discussions and feedback from Prof. Roy Chantrell, Dr. Ondrej Hovorka, and Dr. Lucía Gutiérrez. This work used the computational facilities at the Centro de Supercomputación de Galicia (CESGA). D.S. acknowledges financial support from the Spanish *Agencia Estatal de Investigación* (project PID2019-109514RJ-100). This research was partially supported by the Xunta de Galicia, Program for Development of a Strategic Grouping in Materials

- [1] K. Wu, D. Su, J. Liu, R. Saha, and J.-P. Wang, *Nanotechnology* **30**, 502003 (2019).
- [2] M. Colombo, S. Carregal-Romero, M. F. Casula, L. Gutiérrez, M. P. Morales, I. B. Bohm, J. T. Heverhagen, D. Prosperi, and W. J. Parak, *Chem. Soc. Rev.* **41**, 4306 (2012).
- [3] D. Ling and T. Hyeon, *Small* **9**, 1450 (2013).
- [4] F. Soetaert, P. Korangath, D. Serantes, S. Fiering, and R. Ivkov, *Adv. Drug Deliv. Rev.* (2020), 10.1016/j.addr.2020.06.025.
- [5] E. C. Abenojar, S. Wickramasinghe, J. Bas-Concepcion, and A. C. S. Samia, *Progr. Nat. Sci. Mater. Int.* **26**, 440 (2016).
- [6] M. E. Fortes Brollo, A. Domínguez-Bajo, A. Tabero, V. Domínguez-Arca, V. Gisbert, G. Prieto, C. Johansson, R. Garcia, A. Villanueva, M. C. Serrano, and M. P. Morales, *ACS Appl. Mater. Interfaces* **12**, 4295 (2020).
- [7] N. D. Thorat, R. A. Bohara, M. R. Noor, D. Dhamecha, T. Soulimane, and S. A. M. Tofail, *ACS Biomater. Sci. Eng.* **3**, 1332 (2017).
- [8] J. M. Rojas, H. Gavilán, V. del Dedo, E. Lorente-Sorolla, L. Sanz-Ortega, G. B. da Silva, R. Costo, S. Perez-Yague, M. Talelli, M. Marciello, M. P. Morales, D. F. Barber, and L. Gutiérrez, *Acta Biomater.* **58**, 181 (2017).
- [9] R. Mejías, P. Hernández Flores, M. Talelli, J. L. Tajada-Herráiz, M. E. Brollo, Y. Portilla, M. P. Morales, and D. F. Barber, *ACS Appl. Mater. Interfaces* **11**, 340 (2019).
- [10] D. Serantes, K. Simeonidis, M. Angelakeris, O. Chubykalo-Fesenko, M. Marciello, M. d. P. Morales, D. Baldomir, and C. Martinez-Boubeta, *J. Phys. Chem. C* **118**, 5927 (2014).
- [11] L. Gutiérrez, L. de la Cueva, M. Moros, E. Mazarío, S. de Bernardo, J. M. de la Fuente, M. P. Morales, and G. Salas, *Nanotechnology* **30**, 112001 (2019).
- [12] P. B. Balakrishnan, N. Silvestri, T. Fernandez-Cabada, F. Marinero, S. Fernandes, S. Fiorito, M. Miscuglio, D. Serantes, S. Ruta, K. L. Livesey, O. Hovorka, R. Chantrell, and T. Pellegrino, *Adv. Mater.* (2020).
- [13] N. A. Usov, *J. Appl. Phys.* **107**, 123909 (2010).
- [14] G. Vallejo-Fernandez and K. O'Grady, *Appl. Phys. Lett.* **103**, 142417 (2013).
- [15] J. S. Andreu, J. Camacho, and J. Faraudo, *Soft Matter* **7**, 2336 (2011).
- [16] A. Satoh, R. W. Chantrell, S.-I. Kamiyama, and G. N. Coverdale, *J. Colloid Interf. Sci.* **181**, 422 (1996).
- [17] C. L. Dennis, K. L. Krycka, J. A. Borchers, R. D. Desautels, J. van Lierop, N. F. Huls, A. J. Jackson, C. Gruettner, and R. Ivkov, *Adv. Funct. Mater.* **25**, 4300 (2015).
- [18] I. Conde-Leboran, D. Baldomir, C. Martinez-Boubeta, O. Chubykalo-Fesenko, M. P. Morales, G. Salas, D. Cabrera, J. Camarero, F. J. Teran, and D. Serantes, *J. Phys. Chem. C* **119**, 15698 (2015).
- [19] C. Munoz-Menendez, D. Serantes, J. M. Ruso, and D. Baldomir, *Phys. Chem. Chem. Phys.* **19**, 14527 (2017).
- [20] L. Gutiérrez, R. Costo, C. Gruttner, F. Westphal, N. Gehrke, D. Heinke, A. Fornara, Q. A. Pankhurst, C. Johansson, S. Veintemillas-Verdaguer, and M. P. Morales, *Dalton Trans.* **44**, 2943 (2015).
- [21] L. Nguyen, V. Oanh, P. Nam, D. Doan, N. Truong, N. Ca, P. Phong, L. Hong, and T. Lam, *J. Nanopart. Res.* **22** (2020).
- [22] D. Niculaes, A. Lak, G. C. Anyfantis, S. Marras, O. Laslett, S. K. Avugadda, M. Cassani, D. Serantes, O. Hovorka, R. Chantrell, and T. Pellegrino, *ACS Nano* **11**, 12121 (2017).
- [23] D. Santiago-Quinones, K. Raj, and C. Rinaldi, *Rheol. Acta* **52**, 719 (2013).
- [24] R. Rosensweig, *J. Magn. Magn. Mater.* **252**, 370 (2002).
- [25] T. Kalwarczyk, N. Ziebac, A. Bielejewska, E. Zaboklicka, K. Koynov, J. Szymański, A. Wilk, A. Patkowski, J. Gapiński, H.-J. Butt, and R. Holyst, *Nano Lett.* **11**, 2157 (2011).
- [26] K. Wang, X. H. Sun, Y. Zhang, T. Zhang, Y. Zheng, Y. C. Wei, P. Zhao, D. Y. Chen, H. A. Wu, W. H. Wang, R. Long, J. B. Wang, and J. Chen, *R. Soc. open sci.* **6**, 181707 (2019).
- [27] K. L. Livesey, S. Ruta, N. R. Anderson, D. Baldomir, R. W. Chantrell, and D. Serantes, *Sci. Rep.* **8**, 11166 (2018).
- [28] G. F. Goya and M. P. Morales, *J. Metast. Nanocryst. Mater.* **20-21**, 673 (2004).
- [29] W. C. Nunes, L. M. Socolovsky, J. C. Denardin, F. Cebollada, A. L. Brandl, and M. Knobel, *Phys. Rev. B* **72**, 212413 (2005).
- [30] D. Balaev, S. Semenov, A. Dubrovskiy, S. Yakushkin, V. Kirillov, and O. Martyanov, *J. Magn. Magn. Mater.* **440**, 199 (2017).
- [31] R. W. Chantrell, N. Walmsley, J. Gore, and M. Maylin, *Phys. Rev. B* **63**, 024410 (2000).
- [32] H. Kachkachi, W. T. Coffey, D. S. F. Crothers, A. Ezzir, E. C. Kennedy, M. Noguès, and E. Tronc, *J. Phys.: Condens. Matter* **12**, 3077 (2000).
- [33] N. A. Usov, *J. Appl. Phys.* **109**, 023913 (2011).
- [34] D. Serantes, D. Baldomir, C. Martinez-Boubeta, K. Simeonidis, M. Angelakeris, E. Natividad, M. Castro, A. Mediano, D.-X. Chen, A. Sanchez, L. Balcells, and B. Martínez, *J. Appl. Phys.* **108**, 073918 (2010).
- [35] For a square loop, the coercive field is equal to the anisotropy field,  $H_C = H_K$ . Thus, since  $H_K = 2K/M_S$ , the area is  $A = (2H_K) * (2M_S) = 8K$ .
- [36] M. Donahue and D. Porter, "Oommf user's guide, version 1.0, interagency report nistir 6376, national institute of standards and technology, gaithersburg, md (sept 1999)," <http://math.nist.gov/oommf> (2018).
- [37] O. Lemcké, "Models finite temperature via a differential equation of the langevin type," [http://www.nanoscience.de/group\\_r/stm-spstm/projects/temperature/download.shtml](http://www.nanoscience.de/group_r/stm-spstm/projects/temperature/download.shtml) (2018).
- [38] N. A. Usov, M. S. Nesmeyanov, and V. P. Tarasov, *Sci. Rep.* **8** (2018), <https://doi.org/10.1038/s41598-017-18162-8>.
- [39] I. Morales, D. Archilla, P. de la Presa, A. Hernando, and P. Marin, *Sci. Rep.* **10** (2020), <https://doi.org/10.1038/s41598-017-18162-8>.
- [40] L.-M. Lacroix, R. B. Malaki, J. Carrey, S. Lachaize, M. Respaud, G. F. Goya, and B. Chaudret, *J. Appl. Phys.* **105**, 023911 (2009).
- [41] C. Munoz-Menendez, I. Conde-Leboran, D. Baldomir, O. Chubykalo-Fesenko, and D. Serantes, *Phys. Chem. Chem. Phys.* **17**, 27812 (2015).
- [42] V. R. R. Aquino, M. Vinícius-Araújo, N. Shrivastava, M. H. Sousa, J. A. H. Coaquira, and A. F. Bakuzis, *J. Phys. Chem. C* **123**, 27725 (2019).
- [43] C. L. Dennis and R. Ivkov, *Int. J. Hyperthermia* **29**, 715 (2013).
- [44] J. Carrey, B. Mehdaoui, and M. Respaud, *Journal of Applied Physics* **109**, 083921 (2011).

- [45] L. Branquinho, M. Carriao, A. Costa, N. Zufelato, M. H. Sousa, R. Miotto, R. Ivkov, and A. F. Bakuzis, *Sci. Rep.* **3**, 2887 (2013).
- [46] A. Tewari and A. Gokhale, *Mater. Sci. Eng. C* **385**, 332 (2004).
- [47] D. Serantes, D. Baldomir, M. Pereiro, C. E. Hoppe, F. Rivadulla, and J. Rivas, *Phys. Rev. B* **82**, 134433 (2010).
- [48] L. Beola, L. Asín, C. Roma-Rodrigues, Y. Fernández-Afonso, R. M. Fratila, D. Serantes, S. Ruta, R. W. Chantrell, A. R. Fernandes, P. V. Baptista, J. M. de la Fuente, V. Grazú, and L. Gutiérrez, *ACS Appl. Mater. Interfaces* **12**, 43474 (2020).
- [49] J. Farauto, J. S. Andreu, and J. Camacho, *Soft Matter* **9**, 6654 (2013).
- [50] A. F. Bakuzis, L. C. Branquinho, L. Luiz e Castro, M. T. de Amaral e Eloi, and R. Miotto, *Adv. Colloid Interface Sci.* **191-192**, 1 (2013).